remote sensing

MDPI

Article

Estimation of Bamboo Forest Aboveground Carbon Using the RGLM Model Based on Object-Based Multiscale Segmentation of SPOT-6 Imagery

Yulong Lv [1], Ning Han [2,3,4,*] and Huaqiang Du [2,3,4]

[1] Anji Forestry Bureau, Anji 313300, China; lvyulong@126.com
[2] School of Environmental and Resources Science, Zhejiang A & F University, Hangzhou 311300, China; duhuaqiang@zafu.edu.cn
[3] State Key Laboratory of Subtropical Silviculture, Zhejiang A & F University, Hangzhou 311300, China
[4] Key Laboratory of Carbon Cycling in Forest Ecosystems and Carbon Sequestration of Zhejiang Province, Zhejiang A & F University, Hangzhou 311300, China
* Correspondence: 20110020@zafu.edu.cn; Tel./Fax: +86-(571)-6374-6363

Abstract: Remote sensing is an important tool for the quantitative estimation of forest carbon stock. This study presents a multiscale, object-based method for the estimation of aboveground carbon stock in Moso bamboo forests. The method differs from conventional pixel-based approaches and is more suitable for Chinese forest management inventory. This research indicates that the construction of a SPOT-6 multiscale hierarchy with the 30 scale as the optimal segmentation scale achieves accurate information extraction for Moso bamboo forests. The producer's and user's accuracy are 88.89% and 86.96%, respectively. A random generalized linear model (RGLM), constructed using the multiscale hierarchy, can accurately estimate carbon storage of the bamboo forest in the study area, with a fitting and test accuracy (R^2) of 0.74 and 0.64, respectively. In contrast, pixel-based methods using the RGLM model have a fitting and prediction accuracy of 0.24 and 0.01, respectively; thus, the object-based RGLM is a major improvement. The multiscale object hierarchy correctly analyzed the multiscale correlation and responses of bamboo forest elements to carbon storage. Objects at the 30 scale responded to the microstructure of the bamboo forest and had the strongest correlation between estimated carbon storage and measured values. Objects at the 60 scale did not directly inherit the forest information, so the response to the measured carbon storage of the bamboo forest was the smallest. Objects at the 90 scale serve as super-objects containing the forest feature information and have a significant correlation with the measured carbon storage. Therefore, in this study, a carbon storage estimation model was constructed based on the multiscale characteristics of the bamboo forest so as to analyze correlations and greatly improve the fitting and prediction accuracy of carbon storage.

Keywords: AGC; bamboo forest; object-based segmentation; RGLM model; SPOT-6

Citation: Lv, Y.; Han, N.; Du, H. Estimation of Bamboo Forest Aboveground Carbon Using the RGLM Model Based on Object-Based Multiscale Segmentation of SPOT-6 Imagery. *Remote Sens.* **2023**, *15*, 2566. https://doi.org/10.3390/rs15102566

Academic Editor: Hubert Hasenauer

Received: 21 March 2023
Revised: 27 April 2023
Accepted: 9 May 2023
Published: 14 May 2023

1. Introduction

The application of remote sensing data in combination with forest resource inventory data is an important way to study the forest carbon sink and its response to global climate change [1–7]. Carbon storage estimation using remote sensing data usually relies on understanding absorption, reflection, and transmission of solar radiation, as well as other associated mechanisms within the vegetation canopy and atmosphere. Using satellite-derived information in combination with field measured biomass, forest carbon estimation models based on image pixels can be used to reveal spatial and temporal variations of forest carbon storage [4]. Generally, forest carbon stock is estimated in "pixels"; however, in China, forest features such as woodland area, stand volume, forest growth, etc. are investigated in "sub-compartments" within the forest management inventory [2]. A "sub-compartment" is

a combination of stands with similar biological characteristics and management features. However, there are often significant differences between adjacent stands [8], making it arduous to match remotely sensed image "pixels" with irregular forest sub-compartments. To overcome this limitation, previous studies converted field survey results to carbon stock per unit area through linear interpolation. However, that approach does not sufficiently account for the non-linear characteristics of the forest biomass spatial distribution and the integrity of the forest structure.

An object-based approach has the capability to gather homogenous pixels into image objects to form a closed area through multiscale segmentation. This allows us to extract species information through the objects' spatial characteristics such as size, shape, and position [2,9,10]. Therefore, within the object-based approach, objects and sub-compartments have a certain degree of consistency that is more realistic with respect to the forest management inventory.

Object-based forest information extraction is achieved through multiscale image segmentation as well as the construction of a multi-level classification hierarchy [11–13]. Multiscale segmentation is a crucial element to object-based technology. Through segmentation using different scales, both large- and small-scale data information can be obtained, and therefore the same image can be expressed at various scales at the same time [14,15]. Moreover, the relationship between the super- and sub-object is analogous to the relationship between a large- and small-scale object, which can overcome many limitations of traditional pixel-based information extraction methods. The combination of object-based technology and multiscale segmentation has been applied in prior studies on forest information extraction [11,16–19], as well as for quantitative estimations of forest parameters [20]. Furthermore, object features derived from different scales can be integrated using the GIS overlay tools.

Remote sensing data have three characteristics: (i) high dimensions, (ii) noise, and (iii) complex collinearity issues between features. All three issues present accuracy challenges to models, especially for traditional statistical models such as multiple linear regression [21,22]. Much previous research has documented that machine learning algorithms such as random forest, support vector machine, artificial neural network, etc., can efficiently improve model performance [23–26]. However, many machine learning algorithms are defined as "black box" models, and although they exhibit promising accuracy, it is different to accurately interpret the intrinsic links between variables and output [27]. In this study, a random generalized linear model (RGLM) was developed to estimate Moso bamboo (*Phyllostachys heterocycla* var. *pubescens*) forest carbon stock. The RGLM integrates the high accuracy of ensemble learning and the variable interpretability of the "forward" selection regression model, which is suitable for satellite-based carbon stock estimation. Therefore, the applicability of RGLM has been extended in this work.

The vegetation indices play an important role in estimating forest biomass, accurately reflecting the growth and richness of forest vegetation [28–30], thereby providing a quantitative indicator of forest carbon stock [31]. The vegetation index can be obtained through remote sensing technology, using remote sensing data from different wavelength ranges, to calculate the vegetation indices. Commonly used vegetation indices include the normalized difference vegetation index (NDVI) [32], the difference vegetation index (DVI) [33], and the ratio vegetation index (RVI) [34], etc. NDVI is the most widely used indicator monitoring vegetation growth status [29,30]; DVI can reflect the growth and health status of vegetation, and has a wide range of applications in agriculture, forestry, environmental monitoring [29]; RVI is a sensitive indicator parameter for green vegetation, which can reflect the dynamic changes in leaf stem biomass and chlorophyll content, and can be used to estimate forest carbon stock [31]. Therefore, the application of vegetation indices in forest carbon stock estimation can not only improve the monitoring ability of forest resources, but also contribute to the scientific management and protection of forests as well.

Bamboo forests are an important forest type in the subtropical region of China; they not only yield economic benefit to farmers, but also have a large potential for carbon

sequestration, which can help mitigate global climate change. Therefore, they have become a research focus in recent years [35–38]. Carbon storage is an important parameter that characterizes the ability of forest sequestration. Much previous work has examined the estimation of carbon stock in bamboo forests at the pixel or sub-pixel scale, and estimation results were impressive [4,39–42]. In this study, we adopt an object-based multi-scale segmentation method to construct a multi-scale hierarchical structure system and extract information on the distribution of bamboo forests, and a multi-scale feature carbon storage model of a Moso bamboo forest is constructed by coupling the irregular sample carbon storage and object-based multi-scale remote sensing features. Therefore, we develop a new method to estimate aboveground carbon (AGC) in Moso bamboo forests by using novel object-based multiscale segmentation techniques based on the Chinese forest management inventory. This method surpasses the traditional carbon storage calculation method based on single scale (pixel scale). The results provide new methods for the satellite-based estimation of forest carbon storage at a larger scale using inventory data.

2. Materials and Methods

2.1. Study Area

Anji County, located in northwest Zhejiang Province, China (119°14′~119°53′E, 30°23′~30°53′N), was selected as the study area (Figure 1). The local climate is characterized as subtropical oceanic, with an annual mean precipitation of 1400 mm and mean temperature of 15.6 °C. Anji County has an undulating topography, with elevation ranging from 500 to 1000 m. There is approximately 6.97 × 10^4 ha of Moso bamboo forest, accounting for 40% of the total forest-covered area in the county. Thus, it has been named the home of the Moso bamboo forest.

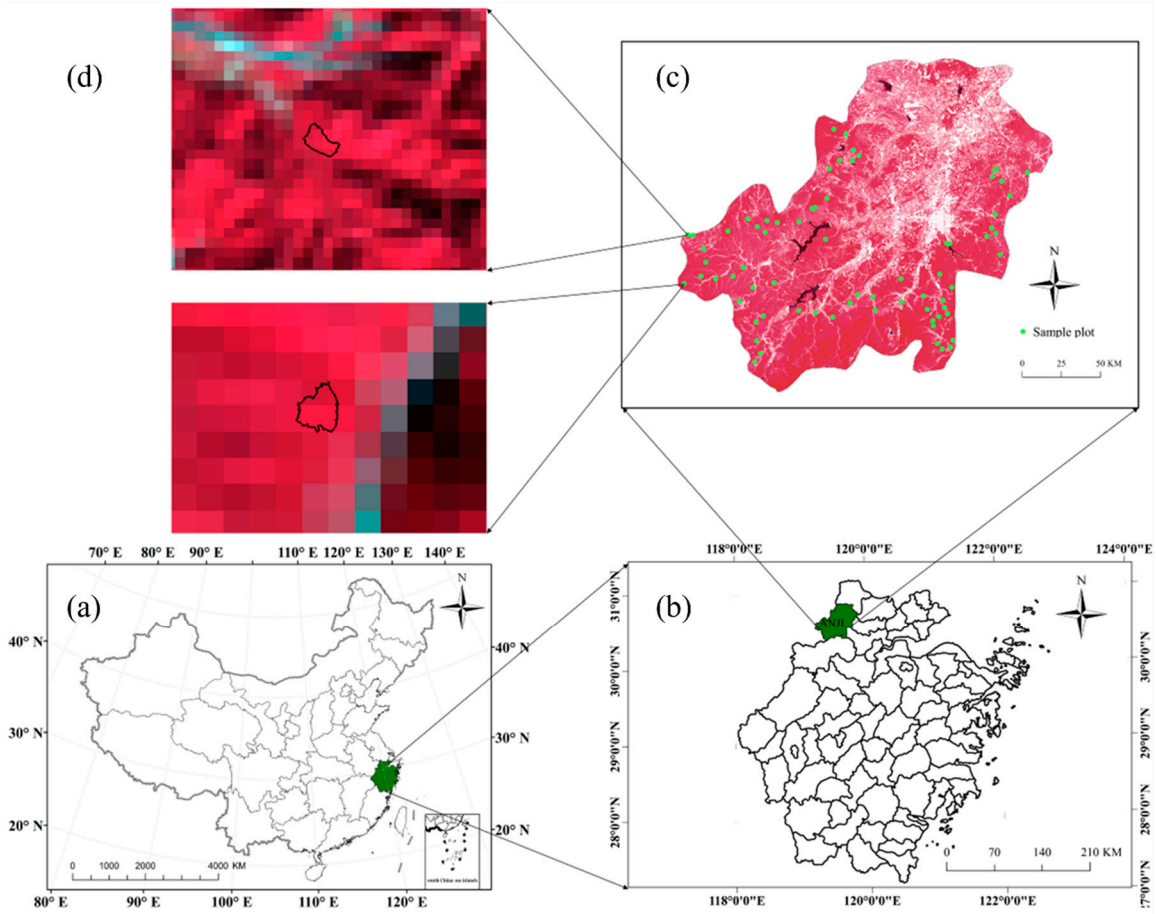

Figure 1. (**a**–**d**) Location of the study area and the distribution of irregular sample plots.

2.2. Research Data and Processing

2.2.1. Remote Sensing Data

Satellite images were taken over the study area by the SPOT-6 satellite on 11 March, 21 July, and 7 October 2014. The SPOT-6 dataset consists of four multispectral bands (blue [0.45–0.52 μm], green [0.53–0.59 μm], red [0.62–0.69 μm], and near-infrared [0.76–0.89 μm]) with a spatial resolution of 6 m × 6 m and a panchromatic band with a resolution of 1.5 m × 1.5 m. All images were geometrically corrected based on a 1:50,000 scale topographic map. The root mean square error (RMSE) was less than 1 pixel, and it was computed using 10 independent ground control points. Subsequently, ortho-rectification using a digital elevation model (DEM) was conducted to reduce topographic effects. Multispectral and panchromatic images were fused to enhance the spatial resolution of the multispectral image to that of the panchromatic image at 1.5 m × 1.5 m. Additionally, the NDVI, DVI, RVI were calculated from the relevant spectral bands.

2.2.2. Field Inventory

Field inventories, which are similar to forest management inventories, were conducted in July 2013 and July 2014. According to a representative sampling and random sampling schemes, a total of 72 irregular sample plots were measured throughout Anji County under varying site conditions, stand density, and management conditions. GPS was also used to record boundaries of those sample plots. In each irregular sample plot, the survey items include the number of Moso bamboo, altitude, slope, canopy density, and management status.

As Moso bamboo is a gramineous species, radial growth stops with the end of high growth, and the biomass per unit area of Moso bamboo has a significant correlation with bamboo quantity. An exponential (Equation (1)) model was applied to demonstrate the relationship between total biomass and number of Moso bamboo in each plot [43]:

$$y = 14.365x^{0.9839} \quad (1)$$

where y is the total dry aboveground biomass (AGB) and x is the total quantity of Moso bamboo in each plot. The exponential model was used to estimate AGB with an accuracy of 0.9643 at a significant level of 0.05. The proportion of bamboo with extremely high values is very small in our study area, and these plots often affect model construction and estimation accuracy. To ensure model performance, a value of 2σ (twice the standard deviation) was used to detect the field sample plots with extremely high values. Twelve plots were identified as outliers because the absolute differences between the AGB and average values are greater than 2σ. Our previous research indicated that the conversion factor from dry biomass to AGC for Moso bamboo is 0.5042 [44]. Thus, the carbon stocks ($Mg \cdot ha^{-1}$) of the bamboo forest for each irregular plot can be successfully calculated. Statistics of the Moso bamboo AGC from the field inventory are showed in Table 1.

Table 1. The descriptive statistics of Moso bamboo forest AGC in 60 sample plots from the field inventory (unit: MgC/ha).

	Sample Size	Min	Max	Mean	SD
Sample plots	60	1.14	10.92	5.72	2.62

2.3. Multiscale Image Segmentation and the Optimal Scale Selection

In the process of image segmentation, scale is a vital parameter, as it affects the size of the segmentation object and the accuracy of the extracted information. In this study, 72 irregular vector polygons were applied as auxiliary data to participate in object-based SPOT-6 data segmentation. Because the size of irregular sample plots varies, only by matching the irregular plots with the segmentation results can the estimation model of the bamboo forest AGC be accurately established.

Five scales were tested to ascertain the most appropriate scale for Moso bamboo mapping and carbon stock estimation. Multispectral bands and NDVI, DVI, and RVI, as well as the filed sample datasets, were used as the input layers for image segmentation. In order to obtain a satisfactory segmentation result, the most effective matching scale with the polygon boundary of irregular plots must be carefully quantified. In this study, segmentation experiments of five-scale parameters were carried out. Table 2 shows the settings for the segmentation parameters. In previous research on information extraction of bamboo distribution, shape criteria were all set to 0.1 [9,11,16,45]. However, because of the inclusion of irregular sample plots in the segmentation, the shape criterion was increased to 0.3 and the color criterion was reduced to 0.7 (shape criterion + color criterion = 1).

Table 2. The segmentation parameters of the SPOT-6 image.

Scale Parameter	Samples Data Used or Not	Shape	Color	Compactness	Smoothness
20	Yes	0.3	0.7	0.5	0.5
30	Yes	0.3	0.7	0.5	0.5
40	Yes	0.3	0.7	0.5	0.5
50	Yes	0.3	0.7	0.5	0.5
60	Yes	0.3	0.7	0.5	0.5

Image segmentation based on the optimal segmentation scale can match irregular plots with the objects, but the object-based method is needed to extract the distribution of bamboo forests from the land-use types. Furthermore, in order to accurately extract bamboo forest information, it is necessary to build a multiscale object hierarchy using the object layer segmented at the optimal scale [45]. In this study, the number of objects that overlapped with irregular plots was used as the criteria for the determination of the optimal segmentation scale.

2.4. Development of the AGC Estimation Model

2.4.1. Variable Selection Using All Subsets Regression Method

Object features, including each object's (1) mean value, (2) standard deviation, and (3) gray-level co-occurrence matrix (GLCM) texture measures, were extracted from every scale level (Table 3). Thus, the corresponding features of 60 irregular samples were extracted. The original object features were filtered using all subsets regression (ASR) to remove redundant features. Compared to the Stepwise Regression (SR) method, which has the disadvantage of "local" optimal variable combination, ASR can traverse all variable combinations and construct multiple linear regression models. ASR finds the "global" optimal variable combination [46] according to the accuracy index of each model, such as determination coefficients (R^2), adjusted R^2 ($adjR^2$), RMSE, or Mallow's C_P. Therefore, the variables selected by ASR are more representative than those from other methods. Since there is a huge number of variables in this study, $adjR^2$ was chosen as the screening index to prevent overfitting during the process of screening variables.

Table 3. Principle of variable selection.

Total Number of Variables (N)	Proportion of Randomly Selected Variables (n/N)
1–10	1
11–300	1.0276–0.00276N
>300	0.2

2.4.2. Introduction of the Random Generalized Linear Model

The RGLM model is a new machine-learning method based on the simple generalized linear model (GLM). This method not only combines the advantages of the "Bagging"

ensemble learning model such as the high precision of the random forest model, but also takes into account the interpretability of variables [27]. The model is summarized in Figure 2.

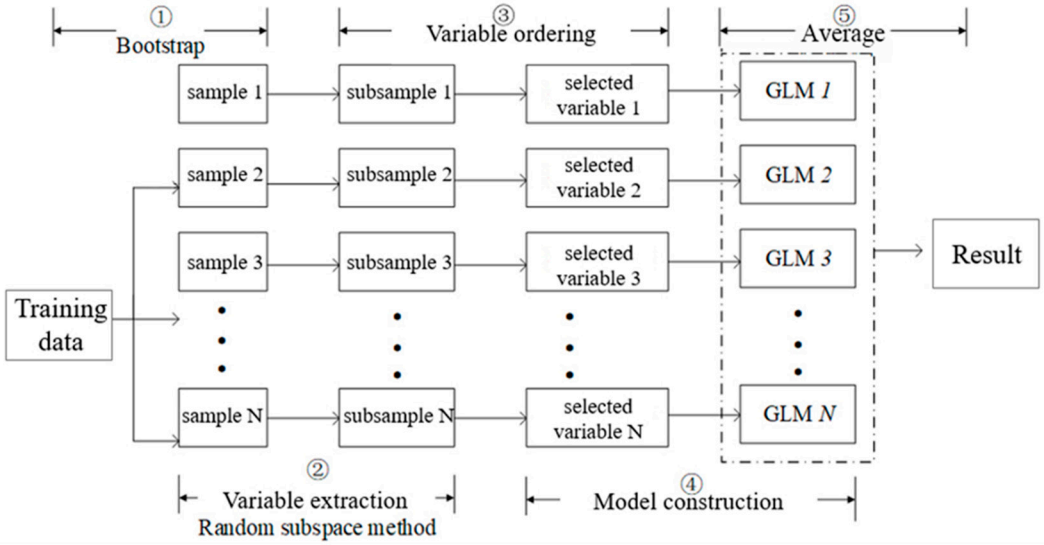

Figure 2. Schematic diagram of the RGLM.

In the first step, N samples were formed using the bootstrap method to train data; in the second step, depending on the number of variables, a number of variables were selected randomly by using the Random Subspace Method [47] to form the subsamples; the rules for randomly selecting variables are shown in Table 3. In this study, there was no significant interaction effects among the eight variables selected, so interactions were not considered.

There were eight variables in the training samples, so all variables were selected. In the third step, the variables were sorted according to the correlations between independent variables and dependent variables and their significance. By default, the first 50 variables after sorting each subsample were used to construct the GLM model. In the fourth step, the "forward selection" method based on the Akaike Information Criterion (AIC) was used to introduce the variables that had sorted and screened subsamples into the GLM model. In the fifth step, the results generated by the GLM model were averaged to obtain the final results [27].

2.5. Accuracy Assessment

The performance of the AGC estimation model was measured by the *RMSE*, R^2, and Lin's Concordance Correlation Coefficient (LCCC), calculated as follows:

$$RMSE = \sqrt{\frac{1}{n}\sum_{i=1}^{n}(p_i - o_i)^2} \quad (2)$$

$$R^2 = 1 - \sum_{i=1}^{n}(p_i - O_i)^2 / \sum_{i=1}^{n}\left(O_i - \overline{O_i}\right)^2 \quad (3)$$

$$LCCC = 2r\sigma_o\sigma_p / \left[{\sigma_o}^2 + {\sigma_p}^2 + (\overline{o} - \overline{p})\right] \quad (4)$$

where o_i and p_i represent the observed value and the modelled value, respectively; σ_o and σ_p represent the standard deviation of the observed and modelled values, respectively; r represents the Pearson correlation coefficient between the observed and modelled value; $\overline{o}$ and $\overline{p}$ represent the mean of the observed and modelled values, respectively. LCCC characterizes the closeness between the best-fit regression and the 1:1 regression line, ranging from 0–1, with larger values indicating better fits [48].

To test the generalization ability of the model, the performance of the RGLM model was evaluated through leave-one-out (LOO) cross-validation. In the LOO procedure [49], one field plot was removed from the input dataset, and then an RGLM model was fitted to the remaining n − 1 plot (where n is the number of field plots). The model was subsequently used to estimate the carbon stock at the removed location. The procedure was repeated n times, once for each field plot. Subsequently, the mean error between the predicted and observed carbon was used as the final accuracy-evaluation standard.

3. Results

3.1. Optimal Segmentation Scale

The five segmentation scales shown in Table 2 were used to segment the SOPT-6 image of Anji County. Table 4 lists the number of objects segmented at different scales and those that overlap with irregular sample plots.

Table 4. Comparison of segmentation results using different scale parameters.

Segmentation Scale	The Number of Objects	The Number of Objects Overlapping with Irregular Samples
20	2,168,849	40
30	1,096,942	68
40	563,176	35
50	375,692	31
60	264,880	26

As illustrated in Table 4, the number of segmentation objects decreased as the scale increased, and the number of objects overlapping with irregular sample plots also changed. When the segmentation scale was set to 30, the number of coincidences reached a maximum value of 68. Figure 3 shows that some irregular samples coincided with objects exactly at the 30 scale. The remaining four irregular sample plots that are not perfect matches with objects were manually adjusted to coincide with the segmented objects. Therefore, a scale of 30 was set as the optimal segmentation scale and the multiscale hierarchy was constructed based on it.

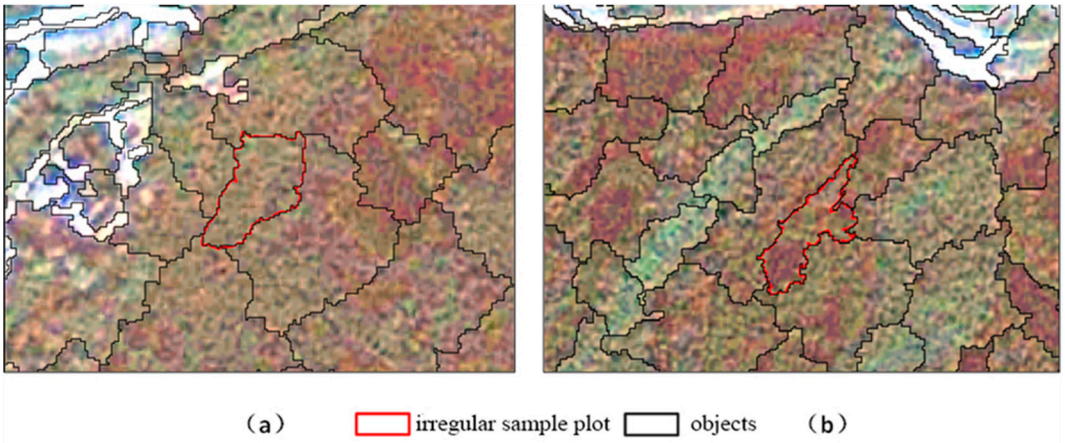

Figure 3. Matching of (**a**) and (**b**) image objects to irregular sample plots at 30 scale.

3.2. Multiscale Hierarchy Construction and Multiscale Object Features Extraction

Hierarchy is an important feature of object-based methods, including object and class hierarchy [11,16]. The object hierarchy is constructed through multiscale image segmentation. Each object layer is created based on its sub-object layer. Therefore, each image object can clearly know its contextual relationships, such as neighbor, super- or sub-objects. The class hierarchy is constructed based on object hierarchy, and the classification

results at a certain scale can serve as contextual features that can be transmitted to the corresponding super- or sub-objects at another scale. In this study, a scale of 30 was set as the optimal segmentation scale; carbon stock estimation was conducted at this scale. Multiscale hierarchy was constructed on a basis of scale 30; two other levels were created above it for extracting the multiscale object features.

Based on the objects segmented at scale 30 (L30), two higher scales of 60 (L60) and 90 (L90) were set so as to establish a three-scale hierarchy (Figure 4) for bamboo forest information extraction. Means and standard deviations of four multispectral bands as well as NDVI, DVI, and RVI were extracted at L30, L60, and L90. In addition, the gray level co-occurrence matrix of four multispectral bands were extracted. Three levels were exported as vector layers with their object features and were intersected using the GIS layer overlay tool. There are 30 object features for each scale and thus a total of 90 features, would be used as a potential source of variables for developing models for carbon stock estimation, as shown in Table 5. Overall, 90 object features were integrated into the layer with the scale of 30.

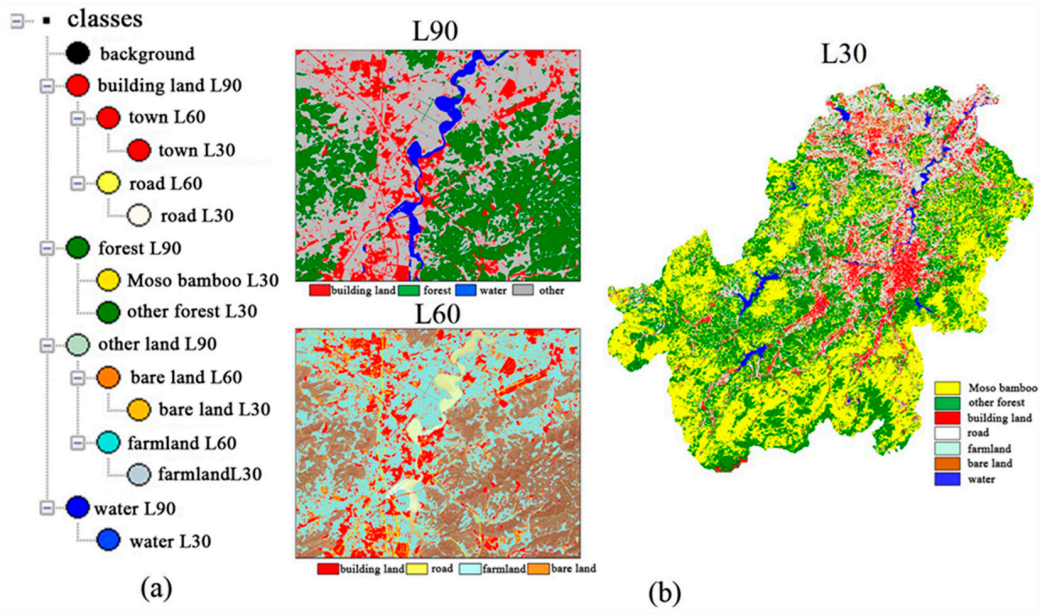

Figure 4. (**a**) Class description in the multiscale hierarchy of image objects; (**b**) classification results at different scales.

Table 5. Description of object-based features.

Feature Number	Feature Name	Feature Meaning	Feature Number	Feature Name	Feature Meaning
F1	L30-GLCMHom4	Texture: NIR homogeneity	F46	L60-Mean7	Mean: RVI
F2	L30-GLCMHom3	Texture: Red homogeneity	F47	L60-Mean6	Mean: DVI
F3	L30-GLCMHom2	Texture: Green homogeneity	F48	L60-Mean5	Mean: NDVI
F4	L30-GLCMHom1	Texture: Blue homogeneity	F49	L60-Mean4	Mean: NIR
F5	L30-GLCMCon4	Texture: NIR Contrast	F50	L60-Mean3	Mean: Red
F6	L30-GLCMCon3	Texture: Red Contrast	F51	L60-Mean2	Mean: Green

Table 5. *Cont.*

Feature Number	Feature Name	Feature Meaning	Feature Number	Feature Name	Feature Meaning
F7	L30-GLCMCon2	Texture: Green Contrast	F52	L60-Mean1	Mean: Blue
F8	L30-GLCMCon1	Texture: Blue Contrast	F53	L60-GLCMStd4	Texture: NIRSD
F9	L30-Std7	SD: RVI	F54	L60-GLCMStd3	Texture: RedSD
F10	L30-Std6	SD: DVI	F55	L60-GLCMStd2	Texture: GreenSD
F11	L30-Std5	SD: NDVI	F56	L60-GLCMStd1	Texture: GreenSD
F12	L30-Std4	SD: NIR	F57	L60-GLCMMean4	Texture: NIRaverage
F13	L30-Std3	SD: Red	F58	L60-GLCMMean3	Texture: Redaverage
F14	L30-Std2	SD: Green	F59	L60-GLCMMean2	Texture: Greenaverage
F15	L30-Std1	SD: Blue	F60	L60-GLCMMean1	Texture: Blueaverage
F16	L30-Mean7	Mean: RVI	F61	L90-GLCMHom4	Texture: NIR homogeneity
F17	L30-Mean6	Mean: DVI	F62	L90-GLCMHom3	Texture: Red homogeneity
F18	L30-Mean5	Mean: NDVI	F63	L90-GLCMHom2	Texture: Green homogeneity
F19	L30-Mean4	Mean: NIR	F64	L90-GLCMHom1	Texture: Blue homogeneity
F20	L30-Mean3	Mean: Red	F65	L90-GLCMCon4	Texture: NIR Contrast
F21	L30-Mean2	Mean: Green	F66	L90-GLCMCon3	Texture: Red Contrast
F22	L30-Mean1	Mean: Blue	F67	L90-GLCMCon2	Texture: Green Contrast
F23	L30-GLCMStd4	Texture: NIRSD	F68	L90-GLCMCon1	Texture: Blue Contrast
F24	L30-GLCMStd3	Texture: RedSD	F69	L90-Std7	SD: RVI
F25	L30-GLCMStd2	Texture: GreenSD	F70	L90-Std6	SD: DVI
F26	L30-GLCMStd1	Texture: GreenSD	F71	L90-Std5	SD: NDVI
F27	L30-GLCMMean4	Texture: NIRaverage	F72	L90-Std4	SD: NIR
F28	L30-GLCMMean3	Texture: Redaverage	F73	L90-Std3	SD: Red
F29	L30-GLCMMean2	Texture: Greenaverage	F74	L90-Std2	SD: Green
F30	L30-GLCMMean1	Texture: Blueaverage	F75	L90-Std1	SD: Blue
F31	L60-GLCMHom4	Texture: NIR homogeneity	F76	L90-Mean7	Mean: RVI
F32	L60-GLCMHom3	Texture: Red homogeneity	F77	L90-Mean6	Mean: DVI
F33	L60-GLCMHom2	Texture: Green homogeneity	F78	L90-Mean5	Mean: NDVI
F34	L60-GLCMHom1	Texture: Blue homogeneity	F79	L90-Mean4	Mean: NIR
F35	L60-GLCMCon4	Texture: NIR Contrast	F80	L90-Mean3	Mean: Red
F36	L60-GLCMCon3	Texture: Red Contrast	F81	L90-Mean2	Mean: Green
F37	L60-GLCMCon2	Texture: Green Contrast	F82	L90-Mean1	Mean: Blue
F38	L60-GLCMCon1	Texture: Blue Contrast	F83	L90-GLCMStd4	Texture: NIRSD
F39	L60-Std7	SD: RVI	F84	L90-GLCMStd3	Texture: RedSD

Table 5. *Cont.*

Feature Number	Feature Name	Feature Meaning	Feature Number	Feature Name	Feature Meaning
F40	L60-Std6	SD: DVI	F85	L90-GLCMStd2	Texture: GreenSD
F41	L60-Std5	SD: NDVI	F86	L90-GLCMStd1	Texture: GreenSD
F42	L60-Std4	SD: NIR	F87	L90-GLCMMean4	Texture: NIRaverage
F43	L60-Std3	SD: Red	F88	L90-GLCMMean3	Texture: Redaverage
F44	L60-Std2	SD: Green	F89	L90-GLCMMean2	Texture: Greenaverage
F45	L60-Std1	SD: Blue	F90	L90-GLCMMean1	Texture: Blueaverage

Note: L30-, L60- and L90- represent feature variables obtained at 30, 60 and 90 scales, respectively; SD represents standard deviation.

3.3. Mapping of the Moso Bamboo Forest

The multiscale hierarchical structure and the class definition of each scale are shown in Figure 4a and Figure 4b, respectively. At the 90 scale, the layer is classified into forest, construction, water, other land, and background. Objects at the 60 scale are sub-objects at the 90 scale. Therefore, at the 60 scale, the construction land at the 90 scale is subdivided into roads and towns, while other land is subdivided into farm and bare land. At the 30 scale, the Moso bamboo forest can be distinguished from forest land, while non-forest objects directly inherit the classification results of the super-objects according to the class hierarchy, including roads, towns, farmland, bare land at the 60 scale, and water at the 90 scale.

155 sample points were randomly generated to construct a classification confusion matrix to evaluate results; overall accuracy was 83.87%, and the Kappa index was 0.8005. The detection of the Moso bamboo forest was satisfactory, with a producer's accuracy of 88.89% and user's accuracy of 86.96%. Because classification accuracy is high, characteristics of the bamboo forest in irregular sample plots will be used to construct an estimation model of carbon stock in Anji County.

3.4. Input Variables Selection

The ASR method was used to filter 90 input variables, and the results are shown in Figure 5. The blank area indicates that the corresponding variables are not selected, the green area indicates that the corresponding variables are selected, and the deeper the color, the higher the accuracy of the linear model. When the variables used to develop the multiple linear regression model were F4, F7, F15, F27, F45, F55, F73 and F74, the model had the best performance, with an adjR^2 of 0.70.

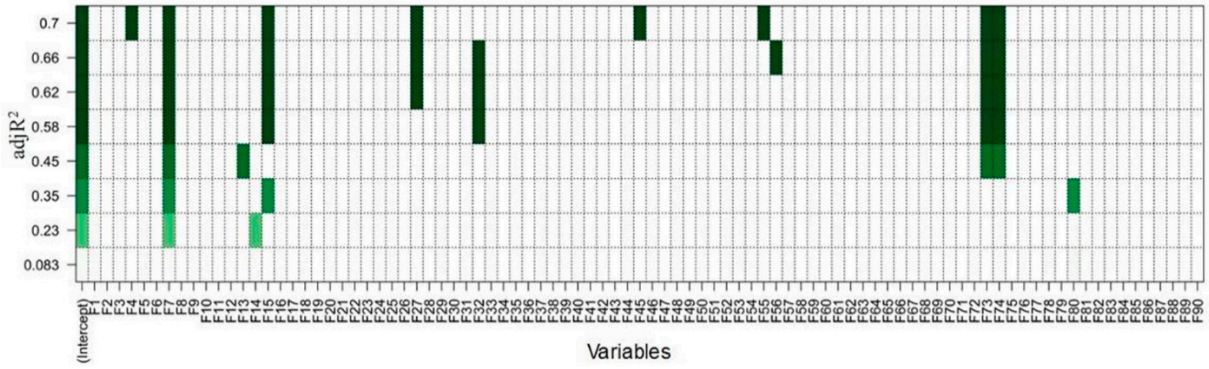

Figure 5. Results of variable selection by ASR.

3.5. The Multiscale Carbon Storage Estimation Model

As shown in Figure 6, the RGLM model produces higher accuracy and less error. In the model training phase, R^2 is 0.74, RMSE is 1.1667 Mg C, and LCCC is 0.84. In the model validation phase, R^2 reduced to 0.64, RMSE increased to 1.3559 Mg C, and LCCC also decreased to 0.78. In general, it shows that the RGLM model has good stability and high precision in estimating the carbon stock of the Moso bamboo forest. The predicted result of carbon stock is shown in Figure 7. The distribution of carbon stock of the Moso bamboo forest generally exhibited high values in the northeast and low in the south. The range of overall carbon stock varies from 0 to 27 MgC/ha. Because of the dense population in central and northern areas of Anji County, the distribution of bamboo forests is relatively small.

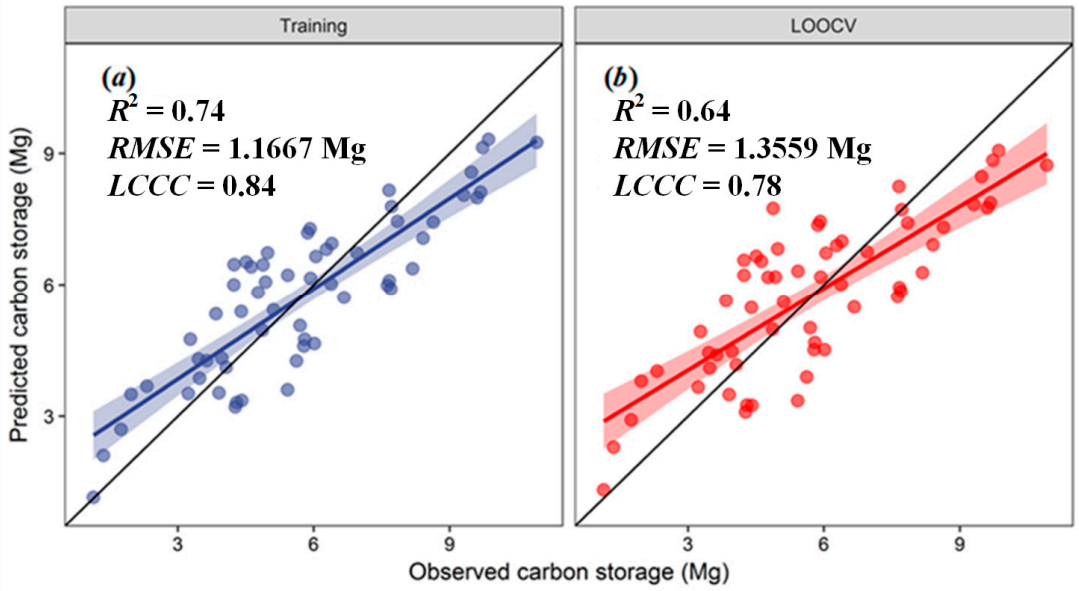

Figure 6. Object-based RGLM Model performance: (**a**) model training, (**b**) LOOCV. Blue and red shadows represent the 95% confidence interval.

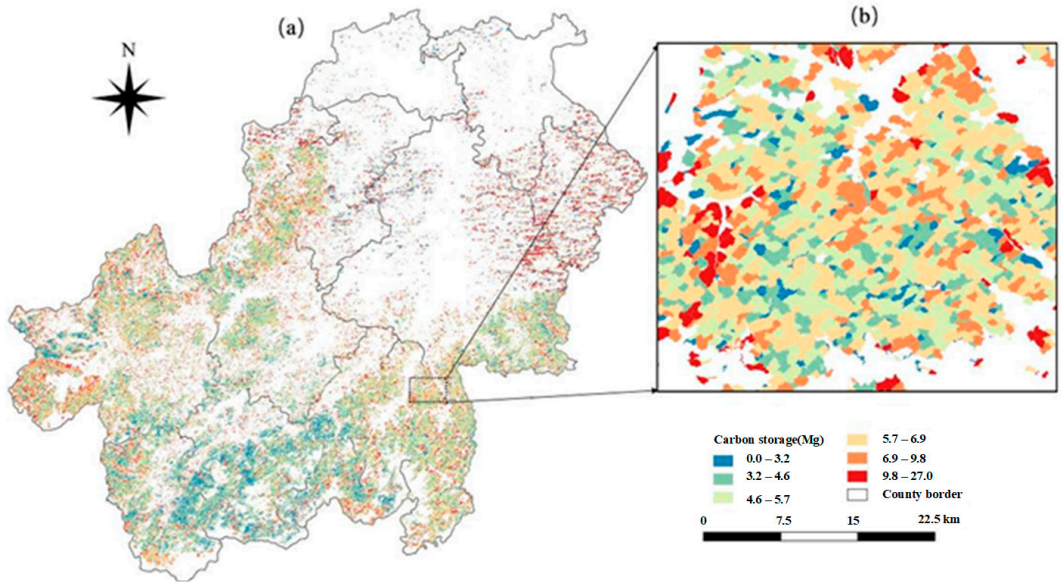

Figure 7. (**a**,**b**) The spatial distribution of object-based carbon storage for the Moso bamboo forest in Anji County.

4. Discussion

This study shows that an AGC estimation model for Moso bamboo forests based on object-based multiscale segmentation performs well in development and validation phases, with R^2 of 0.74 and 0.64, respectively. There is a significant difference in the number of overlapping objects and irregular sample plots under the three single scales of 30, 60, and 90. Zhang et al. also showed that the segmentation scale has a significant impact on the accuracy of object-based classification [50]. On this basis, the study included AGC estimation of the Moso bamboo forest. The model using the features extracted from the multiscale hierarchy greatly improved the accuracy of the AGC estimation in the bamboo forest. Thus, the object-based multiscale model performs well for carbon storage estimation, and the estimated carbon storage of the Moso bamboo forest in Anji County can accurately reflect its spatial distribution.

The primary difference between the object-based AGC estimation model and pixel-based models is that the hierarchical structure can obtain remote sensing information at different scales, which allows carbon storage to be estimated comprehensively according to the multiscale object characteristics. Figure 8 shows the correlations between the predicted carbon storage values at three scales (L30, L60, L90), the object variables, and the measured carbon storage values of the Moso bamboo forest. Feature 7 (F7) and Feature 15 (F15) have a significant response to carbon storage at the 30 scale, and the correlation coefficients between the predicted and measured carbon storage values at the 30 and 90 scales are greater than those at the 60 scale. The main reasons for this are that the optimal segmentation scale of multiscale segmentation is 30 (Table 3), and the sample plots are mainly distributed at the 30 scale; as a result, the four variables (F4, F7, F15, F27) at the 30 scale contain more bamboo forest carbon storage characteristics. A large amount of information for bare and construction land (Figure 4) was primarily integrated at the 60 scale, but the forest land information at the 90 scale was not inherited, so the correlation between the predicted AGC and the measured AGC on this scale was not significant. As the forest information at the 90 scale was inherited directly by the objects at the 30 scale, information was obtained by further subdividing the characteristics on this scale, such that there is a significant correlation between the predicted and measured at the 90 scale, where the objects were regarded as super-objects.

As illustrated in Figure 3, the characteristics of Moso bamboo forest objects at the 60 and 90 scale (super-objects) were inherited directly by the objects at the 30 scale. Therefore, the construction of the multiscale carbon storage estimation model not only considers the micro-structure of the small-scale bamboo forest, but also considers the macro-features of the large-scale bamboo forest, so that it can express bamboo forest characteristics with more semantic information [46]. This means that the carbon stocks of bamboo forests are correlated on multiple scales, and it improves the fitting and prediction accuracy of carbon storage.

In this study, based on the multiscale hierarchy constructed with the optimal segmentation scale (segmentation parameter = 30), the information from the Moso bamboo forest was extracted accurately with a producer's accuracy of 88.89% and user's accuracy of 86.96%. Zhang et al. (2020) and Wei et al. (2023) showed that the object-based method achieved improvement classification performance [5,50]. In comparison, Tan et al. (2021) only utilizes object-based monitoring landslides without optimizing the segmentation scale. The irregular sample plots directly participated in multiscale segmentation at the optimal scale, which ensured that the segmentation objects were consistent with the irregular plots (Figure 3). This lays an important foundation for the construction of an object-based multiscale estimation model for carbon storage in bamboo forests. This solved the challenge of matching ground data with remote sensing pixels and ensured the integrity of the stand structure and remote sensing information. Thus, the estimation accuracy of the carbon stock model is high, and the carbon stock estimation results at the object scale can be presented as a sub-compartment (Figure 7B), which also makes the model more practical. In addition, the construction of a multiscale hierarchy makes the contextual relationship of each image

object very clear, such that the information characteristics of the Moso bamboo forest at different scales can be fully expressed.

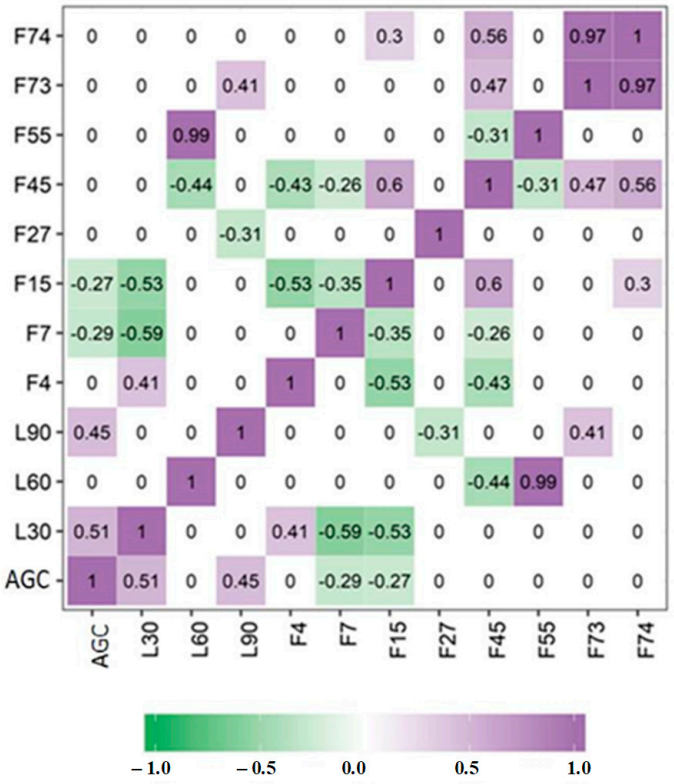

Figure 8. Correlation between the predicted carbon storage values at three scales (L30, L60, L90) with object variables and measured carbon storage values of the Moso bamboo forest.

Pixel-based classification often classifies individual pixels directly according to their spectral information, which is simple to operate but reduces accuracy due to "same objects with different spectra" and "different objects with the same spectra" issues. The object-based method makes the upper layer effectively inherit information from the next layer through multiscale segmentation, making the contextual information relatively coherent. Therefore, objects composed of homogenous pixels have rich information features, such as spectrum, geometry, texture, etc., which can potentially improve classification accuracy [51,52]. In this study, the fitting effect of the AGC model based on pixel and object feature information (F4, F7, F15, F27, F45, F55, F73, F74) was further compared. Results show that the object-based RGLM model performs better than the pixel-based RGLM model in both training and testing phases (Figures 6 and 9), which is consistent with the research results of [25]. Although the *t*-test shows that there is no significant difference between the two residuals ($p > 0.05$), it is obvious that the residual error of the object-based model is more concentrated than that of the pixel-based model, with a range of −2.5~2.5 Mg. In addition, the pixel-based RGLM model has a wide fluctuation range (Figure 10), which further proves that the AGC estimation accuracy can be improved by using object-based multiscale segmentation techniques.

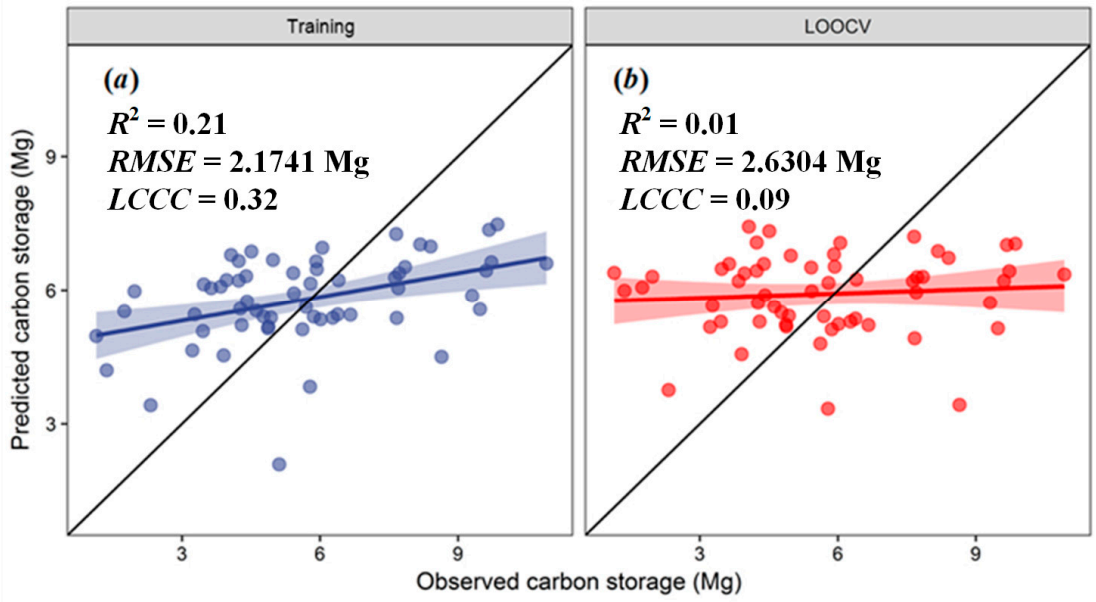

Figure 9. Pixel-based RGLM model performance: (**a**) model training, (**b**) LOO cross validation. Blue and red shadows represent 95% confidence interval.

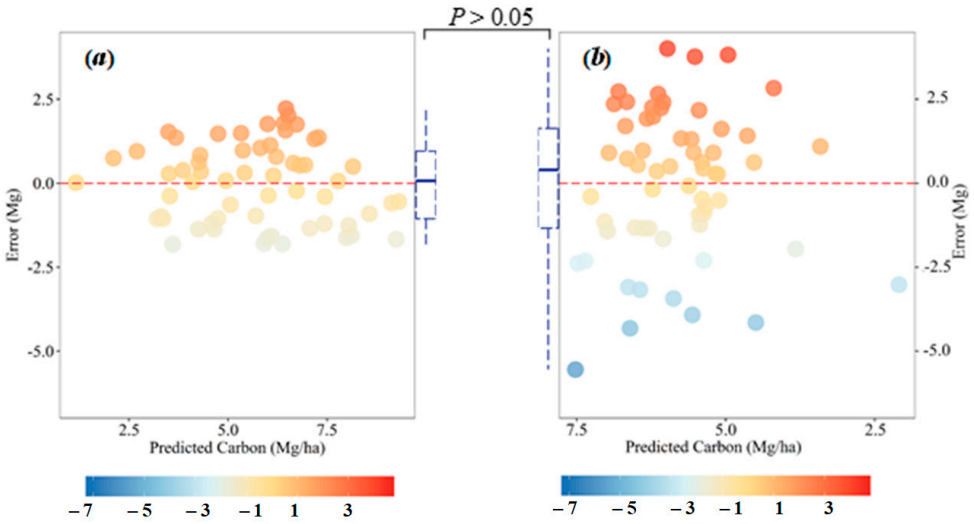

Figure 10. Residual error from the (**a**) object-based RGLM Model, (**b**) pixel-based RGLM model.

5. Conclusions

The study proposes a method for estimating Moso bamboo forest AGC by coupling an object-based multiscale segmentation method and the RGLM model. With 88.89% and 86.96% of producer's and user's accuracy, the result shows that information from the Moso bamboo forest is accurately extracted by constructing a SPOT-6 multiscale hierarchy with the 30 scale as the optimal segmentation scale. The RGLM model based on the multiscale hierarchy can accurately estimate carbon storage of the bamboo forest with a fitting and test accuracy (R^2) of 0.74 and 0.64, respectively. Compared with pixel-based methods using the RGLM model, our model greatly improved the accuracy of AGC estimation in the bamboo forest by using the features extracted from multiscale hierarchy. Thus, the object-based multiscale model performs well for carbon storage estimation, and the estimated carbon storage of the Moso bamboo forest in Anji County can accurately reflect its spatial distribution. However, scale is an important factor in the process of image segmentation, feature extraction, and biomass estimation. Choosing an appropriate segmentation scale has a significant impact on the accuracy of image segmentation, classification, and biomass

estimation. Currently, the best segmentation selection methods are based on statistical analysis of the differences in spectral and other information, which is time-consuming and not intuitive. Therefore, it is necessary to research more intuitive and simple scale segmentation selection methods for different applications in the future.

Author Contributions: Conceptualization, H.D. and N.H.; Data curation, Y.L.; Formal analysis, Y.L. and H.D.; Funding acquisition, H.D.; Investigation, Y.L. and N.H.; Project administration, H.D.; Validation, Y.L. and N.H.; Writing—original draft preparation, Y.L.; Writing—review and editing, H.D. and N.H. All authors have read and agreed to the published version of the manuscript.

Funding: This research was funded by the Leading Goose Project of Science Technology Department of Zhejiang Province (2023C02035), the National Natural Science Foundation (No. 32171785). The authors gratefully acknowledge the support of various foundations. The authors are grateful to the Editor and anonymous reviewers whose comments have contributed to improving the quality of this manuscript.

Data Availability Statement: Not applicable.

Acknowledgments: The authors would like to thank anonymous reviewers for their helpful comments and suggestions.

Conflicts of Interest: The authors declare no conflict of interest.

References

1. Ruusa, M.; Nick, J.; Daniel, N. Improving above ground biomass estimates of Southern Africa dryland forests by combining Sentinel-1 SAR and Sentinel-2 multispectral imagery. *Remote Sens. Environ.* **2022**, *282*, 113232.
2. Ye, S.; Zhu, Z.; Cao, G.F. Object-based continuous monitoring of land disturbances from dense Landsat time series. *Remote Sens. Environ.* **2023**, *287*, 113462. [CrossRef]
3. Powell, S.L.; Cohen, W.B.; Healey, S.P.; Kennedy, R.E.; Moisen, G.G.; Pierce, K.B.; Ohmann, J.L. Quantification of live aboveground forest biomass dynamics with landsat time-series and field inventory data: A comparison of empirical modeling approaches. *Remote Sens. Environ.* **2010**, *114*, 1053–1068. [CrossRef]
4. Wang, J.; Du, H.; Li, X.; Mao, F.; Zhang, M.; Liu, E.; Ji, J.; Kang, F. Remote Sensing Estimation of Bamboo Forest Aboveground Biomass Based on Geographically Weighted Regression. *Remote Sens. Environ.* **2021**, *13*, 2962. [CrossRef]
5. Wei, S.T.; Luo, M.; Zhu, L.F.; Yang, Z. Using object-oriented coupled deep learning approach for typical object inspection of transmission channel. *Int. J. Appl. Earth Observ. Geoinform.* **2023**, *116*, 103137. [CrossRef]
6. Latifi, H.; Fassnacht, F.E.; Hartig, F.; Berger, C.; Hernández, J.; Corvalán, P.; Koch, B. Stratified aboveground forest biomass estimation by remote sensing data. *Int. J. Appl. Earth Obs. Geoinf.* **2015**, *38*, 229–241. [CrossRef]
7. Su, Y.; Guo, Q.; Xue, B.; Hu, T.; Alvarez, O.; Tao, S.; Fang, J. Spatial distribution of forest aboveground biomass in china: Estimation through combination of spaceborne lidar, optical imagery, and forest inventory data. *Remote Sens. Environ.* **2016**, *173*, 187–199. [CrossRef]
8. Kang, X. *Forest Resource Management*; China Forestry Publishing House: Beijing, China, 2001.
9. Sun, X.; Du, H.; Han, N.; Ge, H.; Gu, C. Multi-scale segmentation, object-based extraction of moso bamboo forest from spot5 imagery. *Sci. Silv. Sin.* **2013**, *49*, 80–87.
10. Ming, Q.; Miao, L.J.; Zhou, Z.Q.; Song, J.J.; Dong, Y.P.; Yang, X. Task interleaving and orientation estimation for high-precision oriented object detection in aerial images. *ISPRS J. Photogramm. Remote Sens.* **2023**, *196*, 241–255. [CrossRef]
11. Tan, Q.L.; Guo, B.; Hu, J.; Dong, X.F.; Hu, J.P. Object-oriented remote sensing image information extraction method based on multi-classifier combination and deep learning algorithm. *Pattern Recognit. Lett.* **2021**, *141*, 32–36. [CrossRef]
12. Han, N.; Wang, K.; Yu, L.; Zhang, X. Integration of texture and landscape features into object-based classification for delineating torreya using ikonos imagery. *Int. J. Remote Sens.* **2012**, *33*, 2003–2033. [CrossRef]
13. Pagot, E.; Pesaresi, M.; Buda, D.; Ehrlich, D. Development of an object-oriented classification model using very high resolution satellite imagery for monitoring diamond mining activity. *Int. J. Remote Sens.* **2008**, *29*, 499–512. [CrossRef]
14. Zhou, W.Q.; Huang, G.L.; Troy, A.; Cadenasso, M.L. Object-based land cover classification of shaded areas in high spatial resolution imagery of urban areas: A comparison study. *Remote Sens. Environ.* **2009**, *113*, 1769–1777. [CrossRef]
15. Mallinis, G.; Koutsias, N.; Tsakiri-Strati, M.; Karteris, M. Object-based classification using quickbird imagery for delineating forest vegetation polygons in a mediterranean test site. *ISPRS J. Photogramm. Remote Sens.* **2008**, *63*, 237–250. [CrossRef]
16. Han, N.; Du, H.; Zhou, G.; Sun, X.; Ge, H.; Xu, X. Object-based classification using spot-5 imagery for moso bamboo forest mapping. *Int. J. Remote Sens.* **2014**, *35*, 1126–1142. [CrossRef]
17. Yiming, F.; Zheng, D.; Zhi, C.; Yao, A.; Gao, Z. Desertification land information extraction based on object-oriented classification method. *Sci. Silv. Sin.* **2013**, *49*, 126–133.
18. Ke, Y.; Quackenbush, L.J.; Im, J. Synergistic use of quickbird multispectral imagery and lidar data for object-based forest species classification. *Remote Sens. Environ.* **2010**, *114*, 1141–1154. [CrossRef]

19. Zaki, N.A.M.; Latif, Z.A.; Suratman, M.N. Modelling above-ground live trees biomass and carbon stock estimation of tropical lowland dipterocarp forest: Integration of field-based and remotely sensed estimates. *Int. J. Remote Sens.* **2018**, *39*, 2312–2340. [CrossRef]
20. Chubey, M.S. Object-based analysis of ikonos-2 imagery for extraction of forest inventory parameters. *Photogramm. Eng. Remote Sens.* **2006**, *72*, 383–394. [CrossRef]
21. Zhang, L.; Wang, L.; Zhang, X.; Liu, S.; Sun, P.; Wang, T. The basic principle of random forest and its applications in ecology: A case study of pinus yunnanensis. *Acta Ecol. Sin.* **2014**, *34*, 650–659.
22. Lopatin, J.; Dolos, K.; Hernández, H.J.; Galleguillos, M.; Fassnacht, F.E. Comparing generalized linear models and random forest to model vascular plant species richness using lidar data in a natural forest in central chile. *Remote Sens. Environ.* **2016**, *173*, 200–210. [CrossRef]
23. Dong, L.; Du, H.; Mao, F.; Han, N.; Li, X.; Zhou, G.; Zhu, D.; Zheng, J.; Zhang, M.; Xing, L. Very High Resolution Remote Sensing Imagery Classification Using a Fusion of Random Forest and Deep Learning Technique-Subtropical Area for Example. *IEEE J. Sel. Top. Appl. Earth Obs. Remote Sens.* **2019**, *13*, 113–128. [CrossRef]
24. Li, M.; Im, J.; Quackenbush, L.J.; Liu, T. Forest biomass and carbon stock quantification using airborne lidar data: A case study over huntington wildlife forest in the adirondack park. *IEEE J. Sel. Top. Appl. Earth Obs. Remote Sens.* **2017**, *7*, 3143–3156. [CrossRef]
25. Pham, L.T.H.; Brabyn, L. Monitoring mangrove biomass change in vietnam using spot images and an object-based approach combined with machine learning algorithms. *ISPRS J. Photogramm. Remote Sens.* **2017**, *128*, 86–97. [CrossRef]
26. Yang, R.M.; Zhang, G.L.; Liu, F.; Lu, Y.Y.; Yang, F.; Yang, F.; Yang, M.; Zhao, Y.G.; Li, D.C. Comparison of boosted regression tree and random forest models for mapping topsoil organic carbon concentration in an alpine ecosystem. *Ecol. Indic.* **2016**, *60*, 870–878. [CrossRef]
27. Song, L.; Langfelder, P.; Horvath, S. Random generalized linear model: A highly accurate and interpretable ensemble predictor. *BMC Bioinform.* **2013**, *14*, 5. [CrossRef]
28. Huete, A.R. Vegetation Indices, Remote Sensing and Forest Monitoring. *Geogr. Compass* **2012**, *6*, 513–532. [CrossRef]
29. Xue, J.R.; Su, B.F. Significant Remote Sensing Vegetation Indices: A Review of Developments and Applications. *J. Sens.* **2017**, *2017*, 1353691. [CrossRef]
30. López-Serrano, P.M.; Corral-Rivas, J.J.; Díaz-Varela, R.A.; Álvarez-González, J.G.; López-Sánchez, C.A. Evaluation of Radiometric and Atmospheric Correction Algorithms for Aboveground Forest Biomass Estimation Using Landsat 5 TM Data. *Remote Sens.* **2016**, *8*, 369. [CrossRef]
31. Li, X.J.; Du, H.Q.; Mao, F.J.; Zhou, G.M.; Chen, L.; Xing, L.Q.; Fan, W.L.; Xu, X.J.; Liu, Y.L.; Cui, L. Estimating bamboo forest aboveground biomass using EnKF-assimilated MODIS LAI spatiotemporal data and machine learning algorithms. *Agric. For. Meteorol.* **2018**, *256–257*, 445–457. [CrossRef]
32. Rouse, J.W.; Haas, R.H.; Schell, J.A.; Deering, D.W. 1974. Monitoring Vegetation Systems in the Great Plains with Erts. *NASA Spec. Publ.* **1974**, *351*, 309.
33. Richardson, A.; Wiegand, C. Distinguishing Vegetation from Soil Background Information. *Photogramm. Eng. Remote Sens.* **1977**, *43*, 1541–1552.
34. Jordan, C.F. Derivation of Leaf-Area Index from Quality of Light on the Forest Floor. *Ecology* **1969**, *50*, 663–666. [CrossRef]
35. Lou, Y.P.; Li, Y.X.; Buckingham, K.; Henley, G.; Zhou, G.M. *Bamboo and Climate Change Mitigation*; INBAR: Beijing, China, 2010.
36. Li, P.; Zhou, G.; Du, H.; Lu, D.; Mo, L.; Xu, X.; Shi, Y.; Zhou, Y. Current and potential carbon stocks in moso bamboo forests in china. *J. Env. Manag.* **2015**, *156*, 89–96. [CrossRef]
37. Henley, G.; Lou, Y. *The Climate Change Challenge and Bamboo: Mitigation and Adaptation*; INBAR: Beijing, China, 2009.
38. Zhou, G.; Shi, Y.; Lou, Y.; Li, J.; Yannick, K.; Chen, J.; Ma, G.; He, Y.; Wang, X.; Yu, T. *Methodology for Carbon Accounting and Monitoring of Bamboo Afforestation Projects in China*; INBAR: Beijing China, 2013.
39. Dong, L.; Du, H.; Han, N.; Li, X.; Zhu, D.; Mao, F.; Zhang, M.; Zheng, J.; Liu, H.; Huang, Z. Application of Convolutional neural network on lei bamboo above-ground-biomass (AGB) estimation using Worldview-2. *Remote Sens.* **2020**, *12*, 958. [CrossRef]
40. Zhou, G.; Xu, X.; Du, H.; Ge, H.; Shi, Y.; Zhou, Y. Estimating aboveground carbon of moso bamboo forests using the k nearest neighbors technique and satellite imagery. *Photogramm. Eng. Remote Sens.* **2011**, *77*, 1123–1131. [CrossRef]
41. Shang, Z.; Zhou, G.; Du, H.; Xu, X.; Shi, Y.; Lü, Y.; Zhou, Y.; Gu, C. Moso bamboo forest extraction and aboveground carbon storage estimation based on multi-source remotely sensed images. *Int. J. Remote Sens.* **2013**, *34*, 5351–5368. [CrossRef]
42. Han, N.; Du, H.; Zhou, G.; Xu, X.; Cui, R.; Gu, C. Spatiotemporal heterogeneity of moso bamboo aboveground carbon storage with landsat thematic mapper images: A case study from anji county, china. *Int. J. Remote Sens.* **2013**, *34*, 4917–4932. [CrossRef]
43. Liu, E.; Shi, Y.; Li, Y.; Zhou, G. Carbon sequestration potential of Moso bamboo forest in Zhejiang Province based on the non-spatial structure. *Sci. Silv. Sin.* **2012**, *48*, 9–14.
44. Zhou, G.; Wu, J.; Jiang, P. Effects of different management models on carbon storage in phyllostachys pubescens forests. *J. Beijing Univ.* **2006**, *28*, 51–55.
45. Han, N.; Du, H.; Zhou, G.; Xu, X.; Ge, H.; Liu, L.; Gao, G.; Sun, S. Exploring the synergistic use of multi-scale image object metrics for land-use/land-cover mapping using an object-based approach. *Int. J. Remote Sens.* **2015**, *36*, 3544–3562. [CrossRef]
46. Tavallali, P.; Razavi, M.; Brady, S. A non-linear data mining parameter selection algorithm for continuous variables. *PLoS ONE* **2017**, *12*, e0187676. [CrossRef] [PubMed]

47. Ho, T.K. The random subspace method for constructing decision forests. *IEEE Trans. Pattern Anal. Mach. Intell.* **1998**, *20*, 832–844.
48. Lin, L.I. A concordance correlation coefficient to evaluate reproducibility. *Biometrics* **1989**, *45*, 255. [CrossRef]
49. Calvão, T.; Palmeirim, J.M. Mapping mediterranean scrub with satellite imagery: Biomass estimation and spectral behaviour. *Int. J. Remote Sens.* **2004**, *25*, 3113–3126. [CrossRef]
50. Zhang, C.; Yue, P.; Tapete, D.; Shangguan, B.; Wang, M.; Wu, Z. A multi-level context-guided classification method with object-based convolutional neural network for land cover classification using very high resolution remote sensing images. *Int. J. Appl. Earth Observ. Geoinform.* **2020**, *88*, 102086. [CrossRef]
51. Li, X.; Meng, Q.; Wang, C.; Liu, M.; Zheng, L.; Wang, K. A hybrid model of object-oriented and pixel based classification of remotely sensed data. *J. Geo-Inf. Sci.* **2013**, *15*, 744–751. [CrossRef]
52. Walker, J.S.; Blaschke, T. Object-based land-cover classification for the phoenix metropolitan area: Optimization vs. Transportability. *Int. J. Remote Sens.* **2008**, *29*, 2021–2040. [CrossRef]